True blue InGaN laser for pico size projectors

U. Strauß[+*], S. Brüninghoff[+], M. Schillgalies[+], C. Vierheilig[#], N. Gmeinwieser[+], V. Kümmler[+], G. Brüderl[+], S. Lutgen[+], A. Avramescu[+], D. Queren[+], D. Dini[+], C. Eichler[+], A. Lell[+], U. T. Schwarz[#]

[+] OSRAM Opto Semiconductors GmbH, Leibnizstrasse 4, 93055 Regensburg, Germany
[#] Institute of Experimental and Applied Physics, University of Regensburg, 93040 Regensburg, Germany

ABSTRACT

Red, green and blue semiconductor lasers are of great interest for full color laser projection. Mobile applications require low power consumption and very small laser devices. InGaN lasers are the best choice for the blue color in applications with output power requirements below 100mW: (1) they have much higher wall plug efficiencies than conventional blue frequency doubled diode pumped solid state lasers and (2) they are more compact than semiconductor IR lasers with subsequent second harmonic generation.

We present blue InGaN lasers with high efficiency at a power consumption of several 100mW. Excellent epitaxial quality permits low internal losses. Threshold current densities and slope efficiencies are further optimized by improving the facet coating. The laser threshold current is as low as 25mA and the slope efficiency reaches 1W/A. We present a wall plug efficiency of 15% at output power levels of 60mW.

Keywords: InGaN laser, blue laser, projection, pico projection, wall plug efficiency

1. INTRODUCTION

Features like recording and playback of high resolution pictures or video data, accessing the internet and watching mobile TV are already standard features in today's huge variety of mobile handheld devices like PDAs, media players and cell phones. Currently, the small display size is the limitation for taking full advantage of these features. Usually displays of mobile devices are limited by the device size itself and have QVGA (320x240 pixel) or smaller resolution. One solution to overcome this limitation is the use of embedded, add-on or accessory projectors that can provide high resolution and high brightness "carry-on" screens. Mandatory for such projectors are small form factor and low power consumption in combination with sufficient brightness. Looking at the light source, lasers are very well suited to fulfill these system requirements: lasers are small in size and provide superior beam quality. Therefore, directly modulated red, green and blue lasers are the light source of choice especially for scanning beam projectors. The preferred blue light source is an InGaN laser, which has small size and good modulation frequency.

In this paper we investigate wall plug efficiencies (WPE) of InGaN lasers. WPE is an important parameter for all nitride lasers. The strong dependence of lifetime on power consumption is well known.[1, 2] Mobile applications like pico projectors have limited electrical power and users ask for long operation time without external power supply. To meet this demand, our light sources have to operate at low currents. We investigate wall plug efficiencies of InGaN lasers with special focus on 440nm devices for mobile applications with power consumption in the order of 300mW.

[*] corresponding author: uwe.strauss@osram-os.com

Gallium Nitride Materials and Devices III, edited by Hadis Morkoç, Cole W. Litton, Jen-Inn Chyi, Yasushi Nanishi, Euijoon Yoon, Proc. of SPIE Vol. 6894, 689417, (2008) · 0277-786X/08/$18 · doi: 10.1117/12.761720

2. EXPERIMENTAL

Epitaxial layers of (Al,In,Ga)N are subsequently grown on GaN substrates by metal organic vapor phase deposition (MOCVD). GaN substrates of low dislocation density are required to achieve long lifetimes of InGaN laser devices. A 2.9µm thick n-AlGaN cladding and 100nm n-GaN waveguide are deposited on the GaN substrate. The active layers are three InGaN quantum wells followed by a p-AlGaN electron blocking layer, 100nm p-GaN waveguide, 450nm p-AlGaN cladding and 100nm p-GaN contact layer.

Ridge waveguide laser devices are processed in 5 steps on wafer level: deposition of Pt based ohmic p-contact, ridge structuring by reactive ion etching, SiO_2 passivation layers by plasma enhanced chemical vapour deposition, Ti/Pt/Au bond pad. Our self aligned process for structuring ridge widths from 1.5 to 2.5 µm is described elsewhere.[3] Chip structuring is followed by scribing and cleaving of laser bars and facet coating using TiO2/SiO2. Single emitters are separated and they are soldered on TO56 headers.

Laser devices are analyzed by micro photoluminescence after removal of all metal layers. Optical excitation is done with an Ar ion laser at a wavelength of 380nm. The laser beam is focused with microscope optics down to <1 µm. Excitation and luminescence detection are done with same optics. Lateral resolution is below 1 µm. Details are described by Gmeinwieser et al [4] .

3. IMPROVEMENT OF INTERNAL EFFICIENCIES

In a first step we look at the recombination processes in the InGaN quantum wells. The experiments are done with 405nm laser structures. However, the results are valid for InGaN lasers in general.

The wall plug efficiency of a laser at a certain optical output power depends on threshold current, slope efficiency and operating voltage. Hence, all these parameters have to be addressed for improvement. A low threshold current requires a high internal efficiency and low non-radiative recombination rates.

Non-radiative recombination centers in the InGaN quantum wells can be reduced by optimizing the growth parameters and underlying structures for better crystal quality, which have been subject of many publications. Yet, for this work we focus on the influence of background doping levels on recombination rates. Background doping can be caused by diffusion from highly doped regions in the laser structure or contamination during growth. We find that magnesium causes efficient non-radiative centers. Without proper in-situ cleaning steps between epitaxial runs magnesium accumulates in the reactor. Thus, magnesium is a critical candidate for contamination.

Figure 1 compares the thermal quenching of the electro-luminescence signal of two 405nm laser structures with different magnesium background doping levels in the active layers. With a higher magnesium concentration a much faster quenching is observed. We analyze the quenching with the model

$$P(T) = P_0 / [1 + c\,(-E_a / kT)],$$

where $P(T)$ is the temperature dependent EL intensity, P_0 is approximately the maximum intensity, c is a factor proportional to the non-radiative recombination rate, Ea is the activation energy and k is the Boltzmann constant. We find activation energy of 200meV in both samples. This corresponds to the ionization energy of the MgGa-acceptor,[5] confirming magnesium as the source of the non-radiative recombination. Furthermore, comparing the two samples, the concentration of non-radiative centers is one order of magnitude higher in the sample with the background doping of $2x10^{18}$ cm^{-3}, which is derived from the fit parameter c. This means that there is a linear relationship between the concentration of magnesium and non-radiative centers. We conclude that the reason for the EL quenching is the thermal release of bound holes opening up non-radiative recombination channels.

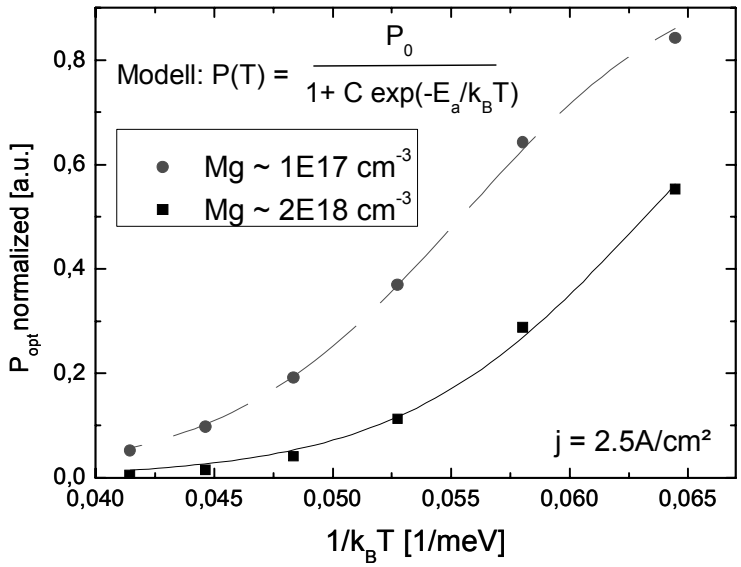

Fig. 1. Comparison of electro-luminescence of 405nm laser structures. Electrical current density is a factor of thousand below laser threshold. The two samples have different magnesium background level in the quantum wells.

Now we investigate whether Mg in the active layers influences laser operation of our 405nm devices. The devices with high Mg background level have worse threshold currents and decreased slope efficiencies. There is also a higher voltage due to the increased operating currents. Our experimental values of wall plug efficiencies of 405nm ridge waveguide lasers are plotted in figure 2. The diagram shows a drop of WPE as a result of Mg impurities.

The high threshold currents are a direct result of the reduced radiative efficiency due to magnesium background doping. Surprisingly, we also found a likewise strong influence on slope efficiency which we attribute to increased internal losses due to absorption and non-radiative recombination in the barriers reducing the injection efficiency. Accordingly, by minimizing magnesium background doping levels it is possible to improve the InGaN-laser's efficiency substantially.

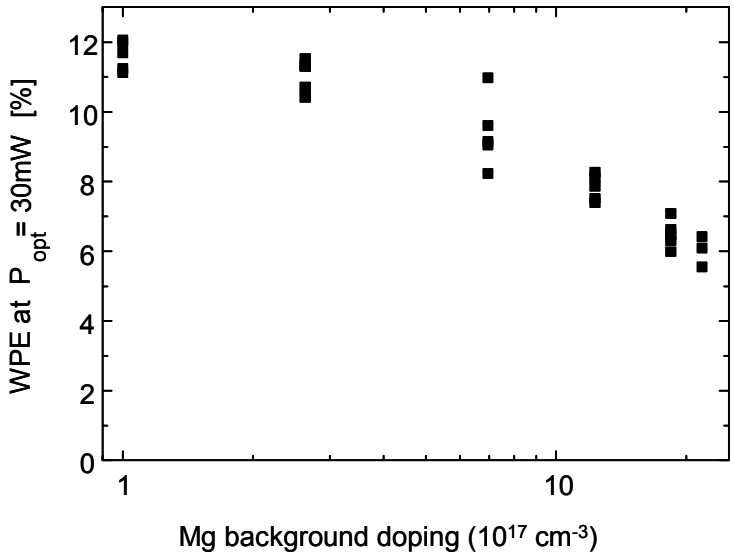

Fig. 2. Experimental data of 405nm laser devices: wall-plug-efficiencies drops to half value for a tenfold increase in magnesium background due to increasing threshold current and decreasing slope efficiency

4. THRESHOLD CURRENT OF LONG WAVELENGTH LASERS

In section 3 we have discussed the improvement of InGaN lasers at 405 nm. At this wavelength, the active layers are InGaN quantum wells with about 8% of In embedded between GaN waveguide layers and AlGaN claddings. At longer wavelengths it becomes more and more complicated to get high efficiencies due to strong increase of laser threshold densities. [6]

We grow long wavelength lasers based on the growth process of 405nm lasers with increased In content of the quantum wells. Quantum wells have In content from 10 to 20% as measured by SIMS. The increase of In content is achieved by lowering the growth temperatures. Stimulated emission is achieved; however, we observed a strong increase of laser threshold at emission wavelengths above 420nm. The results are plotted in figure 3 (closed symbols): threshold current densities at 425nm are already increased by a factor of 6 compared to 405nm devices. A further increase of indium leads to a threshold current density increase by a factor of 9 at emission wavelength of 440nm. Further optimization of growth conditions permits a laser threshold of 440nm laser structures on the same level as 405nm lasers as shown in figure 3 (open symbols).

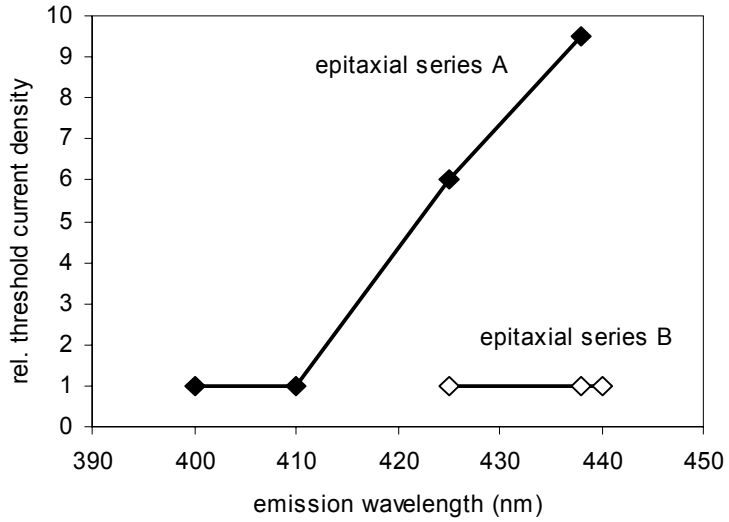

Fig. 3. Threshold current densities of several ridge waveguide lasers. The measured threshold values are normalized to data of 405nm lasers. Epitaxial series A is grown similar to the growth process of 405nm lasers. Series B are epitaxial structures with optimized growth conditions of the InGaN quantum wells.

Several mechanism are discussed as possible root causes for high laser thresholds of long wavelength InGaN lasers: (I) electron-hole separation due to strong piezoelectric fields, (II) point defects of the InGaN quantum wells, (III) indium segregation and (IV) Auger recombination.

In this paper we investigate the lateral homogeneity of the quantum wells. We analyze our lasers by micro-photoluminescence with lateral resolution below 1 µm. The quantum wells are excited resonantly. A plan view of the spatially resolved photoluminescence is plotted in figure 4. We observe local areas with low luminescence intensity. These darker spots are detected at devices with high threshold (epitaxial series A), only. We conclude that In segregation occurs during the epitaxial growth process reducing material quality of the quantum well.

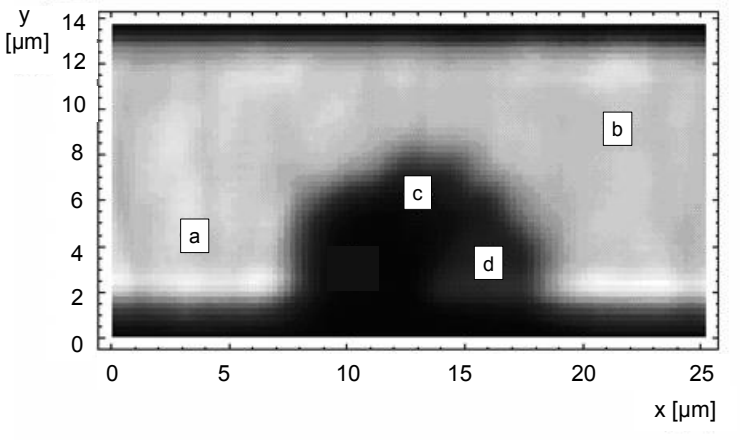

Fig. 4. Intensity map of a spatially resolved photoluminescence measurement. Top view on the laser ridge, metal contacts are removed. The analyzed device belongs to epitaxial series A.

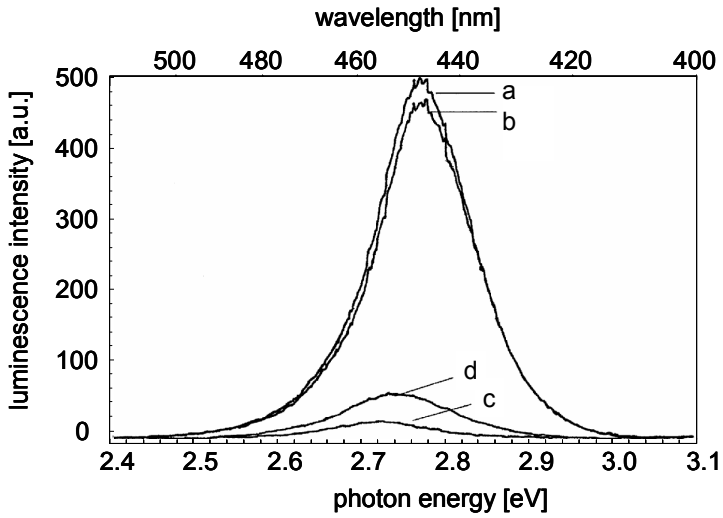

Fig. 5. Local spectra of photoluminescence measurement of epitaxial series A. The spectra belong to four different positions which are marked at figure 4.

In order to investigate the InGaN composition of brighter and darker areas, we analyze local spectra of our photoluminescence mappings as shown in figure 5. Bright areas of the quantum well emit at 450nm, while regions with lower brightness emit at longer wavelengths. We observe a clear dependence of photoluminescence intensity on luminescence wavelength. Therefore we conclude that dark spots are In-rich areas which correlated with In segregation during the epitaxial growth process. Our results of series B show that fine tuning of all growth parameters permits excellent laser thresholds.

5. OPTIMIZED FACET COATINGS

Laser performance like threshold and slope efficiency depends on the reflectivity of the laser facets. We simulated typical lasers with a stripe width of 1.5µm and resonator length of 600µm at a wavelength of 440nm with different facet coatings on the AR-side and constant HR-side-reflectivity of 99%. A self made simulation program is used, utilizing a

linear gain model. Fit parameters are internal losses α_i, injection efficiency η_i, the carrier lifetime τ_s and carrier density in the quantum well n_{th}. Reference data of α_i, η_i, and carrier lifetime are taken from literature. [7, 8, 9]. The simulated output power as a function of electrical current is plotted in figure 6. We observe a weak dependence of threshold current on AR reflectivity, but strong increase of slope efficiencies at lower reflectivity. At an output power of 60mW, required electrical current reduces from 120mA (AR reflectivity of 70%) to 80mA (at AR coating of 30%).

Out of these laser characteristics and the voltage behavior, wall plug efficiencies can be calculated. We use experimental data for the current-voltage dependence. Figure 7 shows calculated wall plug efficiencies, which reach values of 16%, 12% and 8% at AR facet reflectivities of 30%, 50% and 70%, respectively.

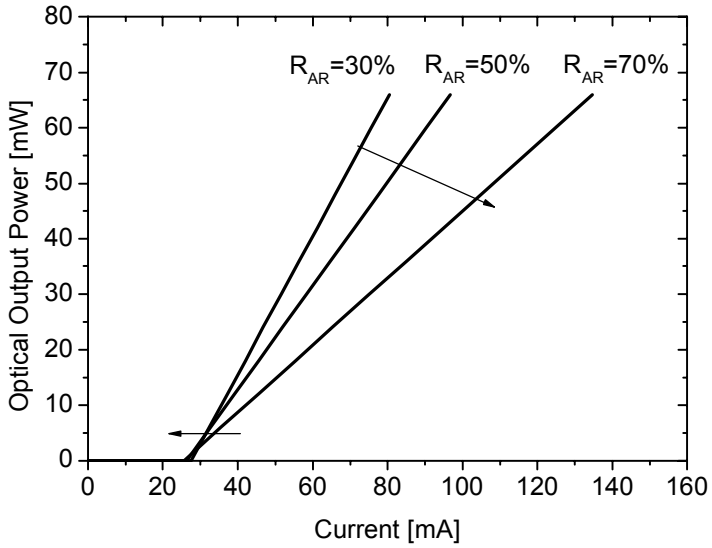

Fig. 6. Electro optical characteristics of 440nm lasers as simulated using three different facet reflectivities. Arrows show the dependence of threshold current densities and slope efficiencies on AR reflectivity, respectively.

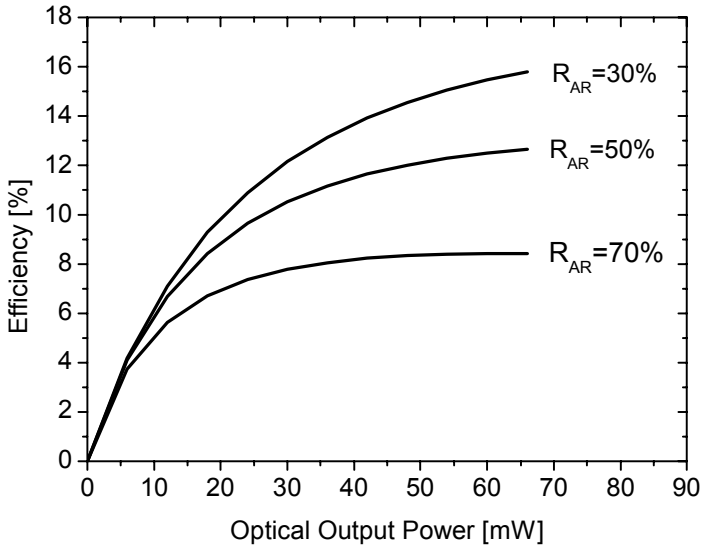

Fig. 7. Simulation of wall plug efficiencies as a function of optical output power. HR facet reflectivities are 99%, AR coatings differ from 30% to 70%.

6. DEVICE PERFORMANCE

Improved epitaxial structures as described in section 3 & 4 are used to process ridge waveguide lasers. The length of the resonator is 600µm, the ridge width is 1.5µm. Best samples reach threshold currents as low as 25mA. The output power increases linearly with current, and slope efficiencies above 1W/A are demonstrated as plotted in figure 8. Best samples reach an optical output power of 30mW at 52mA. The electrical loss at 30mW output power is as low as 250mW, an excellent value for applications with low power consumption.

Figure 9 shows that the wall plug efficiency strongly depends on power level: values of 6.5, 12 and 15% are demonstrated at output power levels of 10, 30 and 60mW, respectively. The strong increase of wall plug efficiencies at power levels below 10mW is related to our low threshold current of about 25mA. Our high slope efficiencies dominate WPE at power levels above 50mW. To our knowledge, efficiencies up to 15% at 60mW are best data reported for blue lasers up to now. [10, 11]

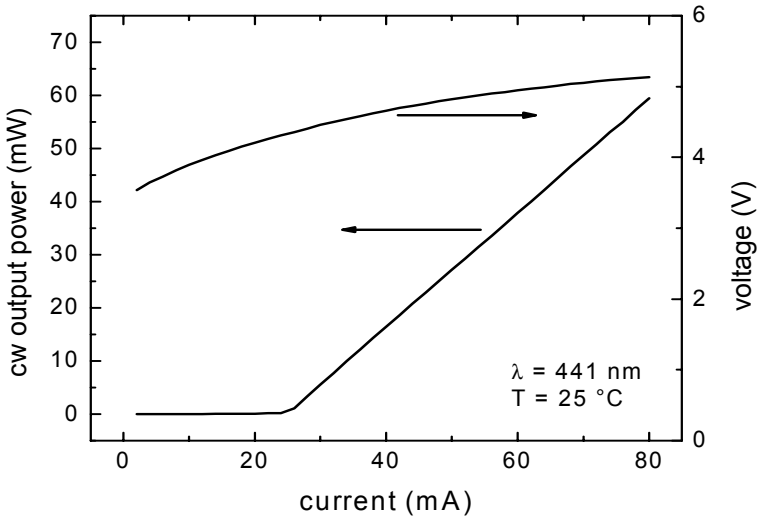

Fig. 8. Experimental data of output power and current-voltage as a function of electrical current. The devices are based on epitaxial series B, emitting at 441 nm.

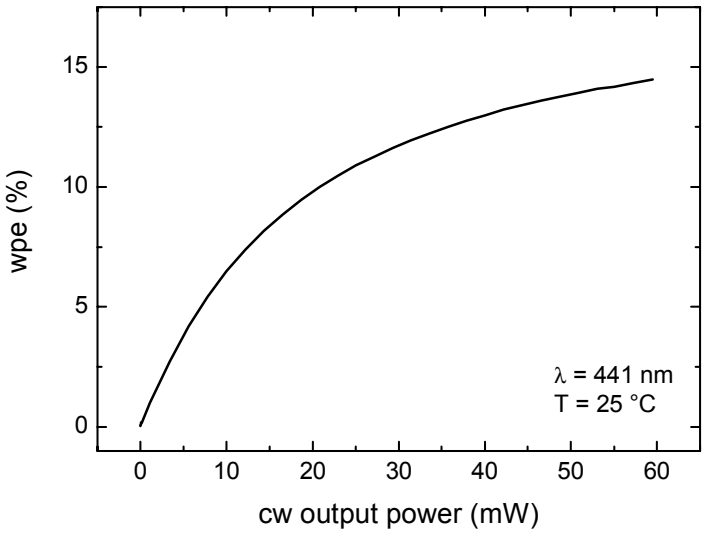

Fig. 9. Experimental data of wall plug efficiency as a function of cw output power. Devices base on epitaxial series B, emitting at 441 nm.

7. CONCLUSION

In conclusion, we report highly efficient true blue lasers for laser projection with low power consumption. We present experimental results indicating that Mg contamination in the active area introduces nonradiative recombination centres, thus deteriorating laser threshold and slope efficiencies. Especially for longer wavelength lasers, indium segregation is observed which led to strongly increased threshold currents. We overcome these effects by fine tuning of the growth conditions and optimizing the facet reflectivities. We demonstrate 440nm blue laser devices with optical output of 30mW, which is suitable for 10lm pico size laser projectors. The overall power consumption of 30mW lasers is as low as 250mW, which is equivalent to wall plug efficiencies of 12%. At higher currents, we achieved laser diodes with wall plug efficiencies up to 15% at 60mW output power at emission wavelengths of 440nm.

ACKNOWLEDGMENTS

This work uses results of 405nm laser development. The 405nm laser project has been supported by the German Ministry of Research and Education contract numbers 01BS150 and 01BS802A/8.

REFERENCES

[1] S. Tomiya, H. Nakajima, K. Funato, T. Miyajima, K. Kobayashi, T. Hino, S. Kijima, T. Asano, M. Ikeda, Phys. Stat. Sol (a) **188**, 69 (2001)

[2] V. Kümmler, G. Brüderl, S. Bader, S. Miller, A. Weimar, A. Lell, V. Härle, U.T. Schwarz, N. Gmeinwieser, W. Wegscheider, Phys. Stat. Sol (a) **194** ,419 (2002)

[3] A C. Rumbolz, G. Bruederl, A. Leber, C. Eichler, M. Furitsch, A. Avramescu, A. Miler, A. Lell, U. Strauss, V. Haerle, Phys. Stat. Sol. (a) **203**, 1792 (2006)

[4] N. Gmeinwieser, P. Gottfriedsen, U.T. Schwarz, W. Wegscheider, R. Clos, A. Krtschil, A. Weimar, G. Brüderl, A. Lell, V. Härle, J. Appl. Phys. **98**, 116102 (2005)

[5] M. A. Reshchikov, and H. Morkoç, J. Appl. Phys. 97, 061301 (2005)

[6] S. Nagahama, T. Yanamoto, M. Sano, T. MukaiJpn. J. Appl. Phys. **40**, 3075 (2001)

[7] U.T. Schwarz, H. Braun, Proc. of SPIE **6485**, 648506 (2007)

[8] B. Witzigmann, V. Laino, M. Luiser, U.T. Schwarz, G. Feicht, W. Wegscheider, K. Engl, M. Furitsch, A. Leber, A. Lell, V. Härle, Appl. Phys. Let. 88, 021104 (2006)

[9] S. Nakamura, IEEE Quantum Electr. 4, 483 (1998)

[10] H. Y. Ryu, H. K. Ha, S. N. Lee, T. Jang, H. K. Kim, J. H. Chae, K. S. Kim, K. K. Choi, J. K. Son, H. S. Paek, Y. S. Sung, T. Sakong, O. H. Nam, Y. S. Park, APL 89, 031122 (2006)

[11] H. Y. Ryu, K. H. Haleem, S. N. Lee, T. Jang, J. K. Son, H. S. Paek, Y. S. Sung, H. K. Kim, K. S. Kim, O. H. Nam, Y. S. Park, J. I. Shim, IEEE Photonics technology letters 19, 1717-1719 (2007)